

**OPEN ACCESS**

## Identifying Defects in Li-Ion Cells Using Ultrasound Acoustic Measurements

To cite this article: James B. Robinson *et al* 2020 *J. Electrochem. Soc.* **167** 120530

View the [article online](#) for updates and enhancements.



The banner features a background of a globe with a grid overlay. On the left, there are three circular logos: the ECS logo, the Electrochemical Society logo, and the Korean Electrochemical Society logo. The central text reads: "Joint International Meeting PRiME 2020 October 4-9, 2020". Below this, a blue bar contains the text "Attendees register at NO COST!". On the right side, there is a large logo for "PRiME PACIFIC RIM MEETING ON ELECTROCHEMICAL AND SOLID STATE SCIENCE 2020". At the bottom right, a blue bar contains the text "REGISTER NOW" with a right-pointing arrow.



## Identifying Defects in Li-Ion Cells Using Ultrasound Acoustic Measurements

James B. Robinson,<sup>1,2,z</sup> Rhodri E. Owen,<sup>1,2</sup> Matt D. R. Kok,<sup>1,2</sup> Maximilian Maier,<sup>1</sup> Jude Majasan,<sup>1</sup> Michele Braglia,<sup>3</sup> Richard Stocker,<sup>3</sup> Tazdin Amietszajew,<sup>4</sup> Alexander J. Roberts,<sup>4,\*</sup> Rohit Bhagat,<sup>4</sup> Duncan Billsson,<sup>5</sup> Jarred Z. Olson,<sup>6</sup> Juyeon Park,<sup>6,\*</sup> Gareth Hinds,<sup>6,\*</sup> Annika Ahlberg Tidblad,<sup>7,8</sup> Dan J. L. Brett,<sup>1,2</sup> and Paul R. Shearing<sup>1,2</sup>

<sup>1</sup>Electrochemical Innovation Lab, Department of Chemical Engineering, UCL, London, WC1E 7JE, United Kingdom

<sup>2</sup>The Faraday Institution, Quad One, Harwell Science and Innovation Campus, Didcot, OX11 0RA, United Kingdom

<sup>3</sup>HORIBA MIRA Ltd., Watling Street, Nuneaton, Warwickshire, CV10 0TU, United Kingdom

<sup>4</sup>Institute for Future Transport and Cities, Coventry University, Coventry, CV1 5FB, United Kingdom

<sup>5</sup>School of Engineering, University of Warwick, Coventry, CV4 7AL, United Kingdom

<sup>6</sup>National Physical Laboratory, Teddington, Middlesex, TW11 0LW, United Kingdom

<sup>7</sup>Volvo Car Corporation, SE-405 31, Gothenburg, Sweden

<sup>8</sup>The Angstrom Advanced Battery Centre, Department of Chemistry, Uppsala University, SE-751 21 Uppsala, Sweden

Identification of the state-of-health (SoH) of Li-ion cells is a vital tool to protect operating battery packs against accelerated degradation and failure. This is becoming increasingly important as the energy and power densities demanded by batteries and the economic costs of packs increase. Here, ultrasonic time-of-flight analysis is performed to demonstrate the technique as a tool for the identification of a range of defects and SoH in Li-ion cells. Analysis of large, purpose-built defects across multiple length scales is performed in pouch cells. The technique is then demonstrated to detect a microscale defect in a commercial cell, which is validated by examining the acoustic transmission signal through the cell. The location and scale of the defects are confirmed using X-ray computed tomography, which also provides information pertaining to the layered structure of the cells. The demonstration of this technique as a methodology for obtaining direct, non-destructive, depth-resolved measurements of the condition of electrode layers highlights the potential application of acoustic methods in real-time diagnostics for SoH monitoring and manufacturing processes.

© 2020 The Author(s). Published on behalf of The Electrochemical Society by IOP Publishing Limited. This is an open access article distributed under the terms of the Creative Commons Attribution 4.0 License (CC BY, <http://creativecommons.org/licenses/by/4.0/>), which permits unrestricted reuse of the work in any medium, provided the original work is properly cited. [DOI: 10.1149/1945-7111/abb174]



Manuscript submitted May 13, 2020; revised manuscript received August 4, 2020. Published August 31, 2020.

Supplementary material for this article is available [online](#)

The ubiquity of Li-ion batteries across a wide range of sectors has resulted in an increased focus on the safe construction and operation of electronic devices. While catastrophic failure events of Li-ion cells are high profile,<sup>1-4</sup> they are also rare. Despite this, accelerated degradation and failure of batteries can occur due to a range of manufacturing faults including the presence of foreign bodies, misaligned electrodes and poor construction of cells.<sup>5</sup> One of the most noted cases of Li-ion battery failure was that of the Samsung Galaxy Note7 mobile phone battery which resulted in at least 96 reports of battery failure within two months of release.<sup>6,7</sup> The high-profile nature of these battery failures points to the need for a robust and efficient screening process that can be used both on a manufacturing line and as a field-deployable technique. Such a tool should also enable an improved understanding of battery degradation<sup>8</sup> by providing active monitoring of the physical condition or state-of-health (SoH) across the cells full lifecycle. While full recycling of batteries remains challenging, there is increasing interest in the repurposing and reuse of Li-ion batteries in second-life applications. When the capacity and power capability drops so that the battery is no longer fit for purpose in first-life applications (often reported as a 20% drop in initial capacity), there remains substantial economic value both in the materials, which comprise the battery, and in the remaining capacity.

The degradation of battery performance has been shown to correlate with physical changes in the constituent material and internal architecture of the cell. At the electrode particle level, cracking, and the consequently enhanced particle porosity, and dislocation from electronic pathways, has been shown to accelerate ageing in both electrodes.<sup>9-12</sup> This behaviour has also been observed

at larger scales with reports of the cracking of the composite electrode structure being correlated to a drop in cell capacity.<sup>13,14</sup> New, high-throughput, in-line techniques for battery quality assurance (QA) are required; however, at present, this monitoring is typically performed using optical techniques, which may not be sufficiently sensitive to identify sub-surface defects.<sup>15</sup> While not yet capable of achieving the required rates for battery QA, the development of X-ray computed tomography (X-ray CT) techniques has occurred at a remarkable pace; for example Kok et al.<sup>16</sup> have demonstrated the potential for the evaluation of a full battery in 80 s.

In addition to the value of in-line monitoring of manufacturing processes to cell producers, field-deployable techniques enable the routine evaluation of cell SoH. These tools must be comparatively compact, low cost and offer fast and reliable results. One such technology, which has particular promise in this area, is ultrasonic acoustic analysis. The ultrasonic time-of-flight (ToF) technique utilises material interfaces to partially reflect signals transmitted from a point source. Material properties including density, porosity and strain affect the propagation of waves through layers, which, in a battery, can provide access to a number of relevant parameters, including the state-of-charge (SoC), electrode condition and potentially the presence of internal defects. The ability to detect small-scale defects has further potential to supplement current techniques applied to SoH monitoring.<sup>17</sup> While the SoH of batteries remains an ill-defined area, routes to access a SoH metric include the analysis of the rate of change of capacity<sup>18</sup> or the internal resistance.<sup>19</sup> However, this can be complicated by the SoC and temperature of cells, the change of open circuit voltage (OCV) during a cells life and external electrical noise. At present, the degradation of batteries is typically determined through predictive modelling due to the substantial difficulty in monitoring the complex nature of battery degradation, particularly with the SoH being a highly application dependent characteristic. Statistical and model-based methods are

\*Electrochemical Society Member.

<sup>z</sup>E-mail: [j.b.robinson@ucl.ac.uk](mailto:j.b.robinson@ucl.ac.uk)

commonly employed to mitigate these effects<sup>20–23</sup> with predicted performance compared to measured parameters. However, this increases the computational expense of battery management systems (BMSs) and the methods are limited by the accuracy of the predicted behaviour. In contrast to computational approaches, a physical measurement, such as ultrasonic time-of-flight analysis, to determine the SoH of Li-ion batteries has the potential to feed into BMSs and provide degradation and failure information, including forewarning of catastrophic events, in real-time without the need for complex calculations.

Reports of ultrasonic analysis of batteries have increased in number and complexity since initial studies performed by Ohzuku et al.<sup>24</sup> who identified particle cracking during cycling using passive acoustic spectroscopy in a Li/MnO<sub>2</sub> cell. This technique was also applied by Villeveille et al.<sup>25</sup> who used passive acoustic emission spectroscopy to monitor morphological changes in a Li/NiSB<sub>2</sub> cell and identify the growth of the solid electrolyte interphase (SEI) during the first cycle and Rhodes et al. who investigated Si electrodes in cells.<sup>26</sup> Sood et al. advanced this work reporting for the first time a drop in through-cell acoustic transmission with cycling associated with cell swelling/gas formation.<sup>27</sup> This work demonstrated the feasibility of using pulse-echo techniques in Li-ion cells; however, the cell used showed severe degradation at a comparatively low cycle rate, with effective failure of the cell occurring after approximately 75 cycles. Hsieh et al. presented a significant development on this work with operando monitoring of a cell throughout multiple cycles using transmission ultrasonic ToF techniques.<sup>28</sup> This work identified changes in both the reflected and transmitted acoustic profiles associated with the lithiation/delithiation process in the electrodes at low cycling rates. Building on this, model development was undertaken by Davies et al.,<sup>29</sup> who identified key parameters which govern the acoustic signal, including the bulk and shear moduli, and Poisson ratio. Previous work by the authors has highlighted the need for spatially resolved acoustic measurements and also examined the effect of high-rate operation, identifying a method for quantifying the “electrochemical stiffness” induced in materials under these conditions.<sup>30,31</sup> While the majority of published work has investigated the use of ultrasound techniques to monitor reversible, expected changes arising in cells due to cell cycling, a recent report by Bomnier et al. demonstrated the use of the technique to identify Li plating in small pouch cells.<sup>32</sup>

This work presents the validation of spatially resolved acoustic ToF measurements in identifying cm-mm scale faults within custom-built cells. The use of the technique is further demonstrated on a commercial cell to detect a microscale-manufacturing defect, the presence of which is corroborated via X-ray CT.

## Experimental

Bespoke cells were constructed with individual layers of electrode removed to generate defects in the electrode stack. The cells were constructed using 11 graphite negative electrode layers and ten LiNi<sub>0.6</sub>Mn<sub>0.2</sub>Co<sub>0.2</sub>O<sub>2</sub> (NMC, Targray, Quebec, Canada) based positive electrode layers stacked and sealed in a laminated Al pouch. To reduce the risk of Li plating and localised cell shorting, 9.5 g of dimethyl carbonate (DMC, anhydrous, >99%, Sigma Aldrich, Missouri, USA) was used as an analogue for the electrolyte to mimic the acoustic properties of commercial electrolytes without the presence of Li<sup>+</sup> salts. During the construction process, deliberate defects were introduced to the cell with the third negative electrode cut in half and one half removed from the stack in one cell. A second defect was introduced in a second cell by dissolving the active cathode material away from the surface of the current collector using the solvent N-methyl-2-pyrrolidone (NMP, anhydrous, 99.5%, Sigma Aldrich). Commercial Li-ion cells composed of a LiCoO<sub>2</sub> (LCO) positive electrode with a graphite negative electrode were also examined (PL-402248-2C, AA Portable Power Corp., Richmond, CA, USA). Acoustic and X-ray imaging of these cells

were performed at their initial OCV of 3.6 V with subsequent imaging performed at similar conditions.

Ultrasonic ToF measurements of the lab-built Li-ion pouch cell analogue were conducted using an Olympus Focus PX phased array instrument (Olympus Corp., Japan). A 10 MHz 1D linear phased array probe consisting of 64 transducers and an active aperture of 64 mm with an element pitch (centre-to-centre distance between elements) of 1 mm. The probe was fitted with a 0° Rexolite wedge to protect the surface of the transducer. For cell mapping measurements, the active aperture of the probe was reduced to match the width of the cell. Movement along the length of the cell was measured using an Olympus GLIDER 2-axis encoded scanner with the step size set at 1 mm to give a resolution of ca. 1 mm<sup>2</sup>. Elements were pulsed in groups of 16. Analysis of the measured signals was performed using the OmniPC software with visualisation undertaken in Matlab. Further pulse-echo ToF measurements were performed on commercial 400 mAh LiCoO<sub>2</sub>/graphite cells using a Panametrics 5052PR pulse-receiver to excite the ultrasound transducer. The response signal was recorded using the same Panametrics pulse-receiver unit which was in turn connected to a Tektronix TBS 1052-EBU digital oscilloscope. The measurements were taken at a rate of 1 Hz with 64 signals averaged to give the final waveform and minimise the impact of external noise effects. The measurements were obtained with a 1 MHz (Panametrics) transducer with a 12.7 mm diameter at an appropriate drive level to ensure the response signal was not of sufficient amplitude to saturate the receiver. Ultrasonic transmission measurements were obtained by using a second receiving probe (5 MHz, Olympus Corp., Japan) with a diameter of 6.35 mm placed on the opposite side of the cell and connected to the oscilloscope. A uniform pressure between the transducer(s) and cell was maintained by placing a 200 g weight on one transducer prior to all measurements with the receiver transducer placed below this when transmission measurements were obtained. The waveforms were exported from the oscilloscope as a .csv file prior to analysis in Matlab. To facilitate acoustic measurements an ultrasonic couplant (D12 Couplant, Olympus Corp., Japan) was placed between the cells and transducers prior to all measurements.

The internal characteristics of the lab-built cells were identified via X-ray CT, conducted using a Nikon XT-225 instrument (Nikon Metrology, Tring, UK). These scans were obtained at an accelerating voltage of 180 kV and an incident beam power of 18.5 W, using a W target and a 1 mm Cu filter. To minimise artefacts in the image, 3176 projections were obtained for each scan with the geometric magnification of the system resulting in a pixel size of approximately 24.5 μm. Reconstruction of the radiographic images was performed using “Nikon CT Agent” software, which enabled the visualisation of the electrode layers, and current collection tabs within the cell. The commercial cells were imaged using a Zeiss Xradia Versa 520 (Carl Zeiss XRM, Pleasanton, CA, USA) with an accelerating voltage of 80 kV and a total power of 10 W. A total of 1601 projections were collected with a magnification of 0.4× used to obtain a resolution of 7.7 μm. Reconstruction of the acquired images was conducted using proprietary software (“Reconstructor Scout-and-Scan, Zeiss, Carl Zeiss, CA, USA) with visualisation of all reconstructed datasets being performed using Avizo Fire 9.4 (FEI, France).

## Results and Discussion

In order to leverage acoustic techniques in a QA or quality control (QC) process it must be demonstrated that ToF-based techniques can establish a significant and reproducible signal variation between pristine regions and those that contain defects. The interpretation of acoustic ToF signals in Li-ion batteries is governed by a number of factors including the condition and mechanical properties of the constituent materials and the internal architecture of the cell. In a cell under electrochemical load this becomes increasingly challenging due to SoC-dependent variations in electrode properties which affect the speed of sound (*c*) in a

material; most noticeably the Young's modulus ( $E$ ), density ( $\rho$ ) and Poisson ratio ( $\nu$ )<sup>29</sup> as seen in Eq. 1, where  $K$  and  $G$  are the bulk and shear moduli respectively (Eqs. 2 and 3).

$$c = \sqrt{\frac{K + \frac{4}{3}G}{\rho}} \quad [1]$$

$$K = \frac{E}{3(1 - 2\nu)} \quad [2]$$

$$G = \frac{E}{2(1 + \nu)} \quad [3]$$

These considerations are not required when analysing a cell which has been allowed to rest at open circuit, removing any variation in the SoC and consequently the condition of the constituent layers and any potential electrochemical stiffness derived from cycling.<sup>31</sup> Under these circumstances, any change in the ToF will be entirely governed by the physical distance between the interface causing reflections and the transducer. However, in Li-ion batteries, the layered structure provides a number of component ( $i$ ) velocities in each composite material, which must be considered to facilitate appropriate analysis and obtain direct measurements of depth ( $z$ ).

$$\text{ToF} = \sum_{i=1}^{i=n} c_i(\rho, \tau \dots) \cdot z_i \quad [4]$$

While in principle this is a relatively facile calculation, the impact of a large number of factors (which may be spatially variant), including, particle size, density, local electrode composition and tortuosity, provide significant challenges to directly measure thicknesses in real cells. The amplitude of the reflected peaks at an interface is governed by the reflection coefficient ( $R$ ) which indicates the extent to which an incident acoustic wave is reflected. This coefficient depends on the relative acoustic impedance ( $Z$ ) of the two materials at the interface, and is calculated as shown in Eq. 6.

$$Z = \rho c \quad [5]$$

$$R = \left( \frac{Z_2 - Z_1}{Z_1 + Z_2} \right)^2 \quad [6]$$

Despite the complications outlined above, acoustic techniques can provide highly resolved results that can be used to detect changes in well-characterised systems. Employing this approach, acoustic ToF signals can be subtracted from known standards and variations in rectified peak locations can be observed in a two-dimensional map. These changes in peak behaviour may arise due to a range of physical factors in a cell, some of which are outlined in Fig. 1.

The first and most likely cause of a variation in total amplitude over a given ToF range in a Li-ion cell at OCV will be due to a physical shift in the interface location as outlined in Fig. 1a. A shift in the interface towards or away from the transducer caused by electrode layer expansion or contraction will change the measured amplitude of the peak at a given ToF value with the apparent amplitude of the peak decreasing directly as a result. This shift in ToF as a result of cycling has been reported in a number of works<sup>28,31</sup> and can be accounted for in a monitoring system by ensuring a range of ToF values are included in any peak analysis with only the maximum amplitude being assessed. The extent of the range will be determined by the resolution of the measurement; however, it should be sufficient to accommodate slight structural or surface variations, which may manifest over nanosecond timescales. An actual change in the peak amplitude at a given ToF, shown in

Fig. 1b, is unlikely to be measured in a healthy cell at OCV, as this change would require a change in the physical properties of the materials at the interface. A shift in the amplitude for a cell at rest is indicative of a defect in a region located at a prior ToF and is due to the reduced transmission of acoustic waves through the cell. Finally, the absence of a peak (Fig. 1c) would most likely be due to a severe defect in a cell, such as the removal of an electrode layer. The loss of a peak and subsequent features in a waveform is indicative of the presence of a non-acoustically conductive layer, provides a facile method for determining the presence of degradation indicators such as accumulated gas pockets and delamination in cells.

To validate the use of this technique against known defects, the phased array probe was rastered across a cell to provide a scan of the cell in three dimensions, namely,  $x$ ,  $y$  and ToF, corresponding to a thickness, as shown in Fig. 2.

Following the full three-dimensional acoustic scan, individual peaks were examined to understand the spatially variant changes in the waveforms obtained. A consistent delay was applied to the signals to remove the peaks associated with the ringing of the transducers, which were also shifted in ToF due to the presence of the delay block. The total delay applied was consistent across all measurements. To ensure a minor peak shift had not caused any variation, the maximum amplitude over a  $0.4 \mu\text{s}$  range was plotted. Slight variations in the signal amplitude were observed across all peaks due to the packaging of the pouch cell, which allowed slight movement of both the electrode layers and electrolyte. However, when interrogated, a single peak located at ca.  $2.0 \mu\text{s}$  was observed to show an approximately constant amplitude (Region 1) before a sharp deviation from this expected amplitude; seen in Region 2 where the peak amplitude approaches zero. The large change in the gradient of the amplitude is indicative of either a large shift in the peak location or the absence of a peak in this location as described in Figs. 1b, 1c. The peak at  $2.0 \mu\text{s}$  is observed to be the third significant peak in the acoustic signal, suggesting the defect observed occurs in the third layer of the cell, in this instance, corresponding to the removed anode layer in the deliberately constructed cells. This is further corroborated via the reconstructed tomography image shown in Fig. 2c. While there is a region of reduced ToF peak amplitude after the large gradient (Region 2 in Fig. 2b), variations in the measured values can be seen to increase from zero as the raster moves towards the other end of the cell (Region 3). The signal in Region 3 is complicated by the increasing degree of curvature of the cell due to the pressure from the transducer. It can also be seen in the X-ray image (Fig. 2c), that the cell allows movement of the entire electrode region, which contributes to slight variations in the location of peaks. This effect is most likely to occur in Region 2 where the weight of the transducer is not uniform across the surface of the cell due to the removal of the anode layer (seen in Fig. 2c) in a similar manner to an anchoring effect previously reported.<sup>21,22</sup> This boundary region will result in a sudden reduced constriction on the anode layer, which will tend to bend towards the free space due to the pressure of the transducer and the edge of the electrode layer. Measurement in regions where this variation in pressure occurs (i.e. Region 2) is facilitated by the couplant, which is in sufficient quantity to ensure no air gaps are present between the transducer and the cell.

In examining the regions above, it is evident that there is intimate contact between the layers and electrolyte due to the presence of subsequent peaks, which can only be measured in the presence of an acoustically conductive medium. In this instance, propagation is achieved through the liquid DMC electrolyte, which is in excess when compared to industrially formulated pouch or prismatic cells. Deeper examination of individual waveforms from the aforementioned regions provides further evidence that there is a relative change in position of the electrode layers in the cell as seen in Fig. 3.

The variation in signal between Region 1 and 2 is evident across all ToFs in Fig. 3a, with better agreement evident only in the first echo peaks, i.e. those occurring from ca.  $6.9 \mu\text{s}$  onwards. These echo peaks are associated with the waveform passing through the entire

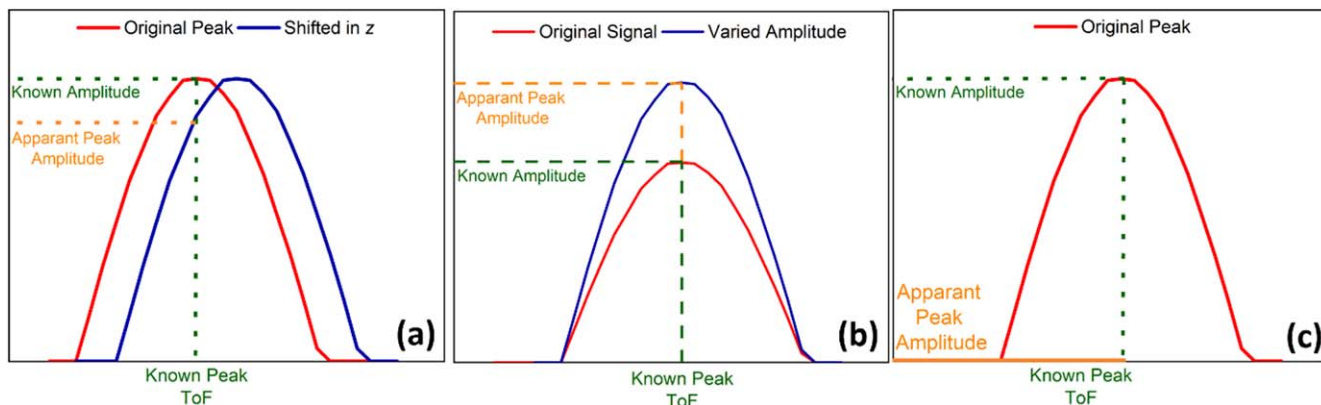


**Figure 1.** A number of potential peak variations in acoustic ToF analysis of Li-ion batteries including (a) a change in measured amplitude due to the interface physically moving in  $z$ , (b) a measured increase in the amplitude due to a change in the ratio of acoustic impedances at a given interface and (c) the complete absence of the interface being measured.

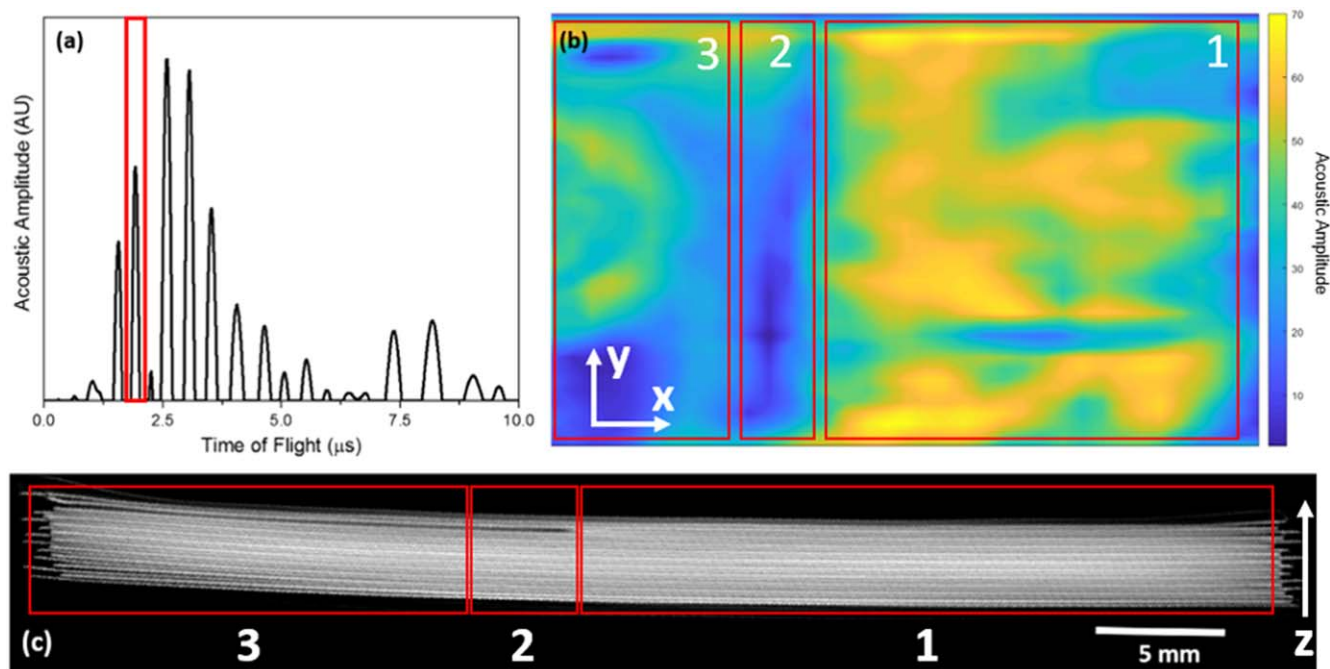


**Figure 2.** Diagnostic analysis of a Li-ion pouch cell with a large anode defect (in this instance one electrode layer removed in one half of the cell) showing (a) a sample acoustic signal from the area without the defect highlighting the third layer within the cell as the peak of interest; (b) a 2D raster of acoustic scans corresponding to the amplitude variations of the peak at ca.  $2.0 \mu\text{s}$  (with a  $0.4 \mu\text{s}$  range applied to account for small ToF shifts) and (c) a reconstructed X-ray CT of the cell confirming the defective region in the cell. Regions are indicated 1, 2 and 3 to aid later discussion.

cell and reflecting off the back of the cell and therefore, when analysing potential movement in the electrode layers in a cell, should be considered in a different manner. In contrast, there is similarity between the peaks in Region 2 and 3 until ca.  $2.0 \mu\text{s}$ . Following this peak, minor variations in the waveforms are evident in each region, suggesting a movement of the component layers before similarity is once again observed from ca.  $4.8 \mu\text{s}$  until the echo peaks are measured at  $6.9 \mu\text{s}$ . The variations in the region  $2.0\text{--}4.8 \mu\text{s}$  begin with the third major peak and suggest that the bending effect noted previously propagates through several layers before the layers are sufficiently constrained due to the pressure applied by the weight of the transducer and the neighbouring electrode layers. It can also be seen that the signal obtained in Region 3 has a more periodic structure, in contrast to the irregular peak locations in Region 2. This suggests that in Region 2 the pressure of the transducer is acting across a sufficiently large area to press the remaining electrode layers together and is not influenced by the “ledge effect” seen in

Region 2. The variations in the individual signals shown in Fig. 3 highlight a challenge in applying single measurements to detect defects which occur over large areas of the cell (i.e. larger than the transducer). The variations also point to the importance of not only applying a uniform weight, but also a consistent force when using single-point measurements as the relative changes in a waveform will not be observed across the cell.

Having validated the technique against large defects (i.e. the absence of an entire electrode layer), the potential use of acoustic spectroscopy as a tool to detect in-electrode defects was examined. Delamination of electrode layers is highly detrimental to cell performance and a predictor of the onset of cell failure.<sup>13,14,16</sup> As a proxy for electrode delamination a region of cathode located in the fourth layer of a cell similar to that discussed previously was removed prior to sealing, with the results shown in Fig. 4.

Once more, it can be seen that spatially resolved pulse-echo imaging can be used to identify defective regions in the electrode.

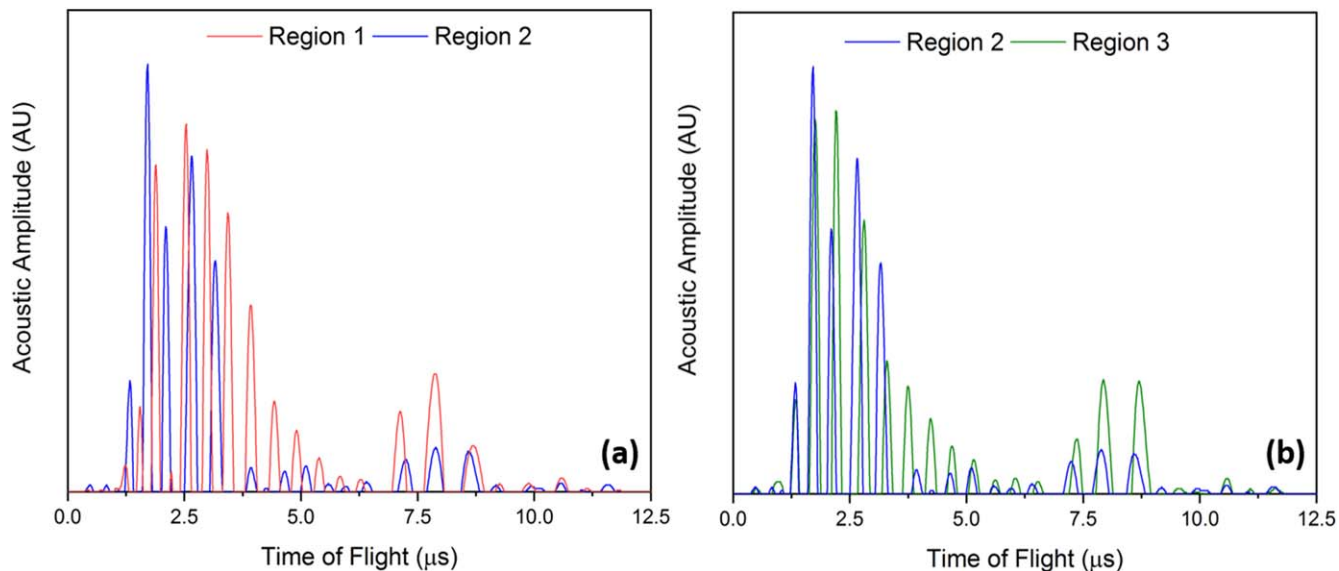


**Figure 3.** Example waveforms highlighting the relative change in displacement between the transducer and electrode layers caused by the ledge effect, showing a large variation throughout the waveforms between Region 1 and 2 and a similarity in waveforms until ca. 2  $\mu\text{s}$  between Region 2 and 3.

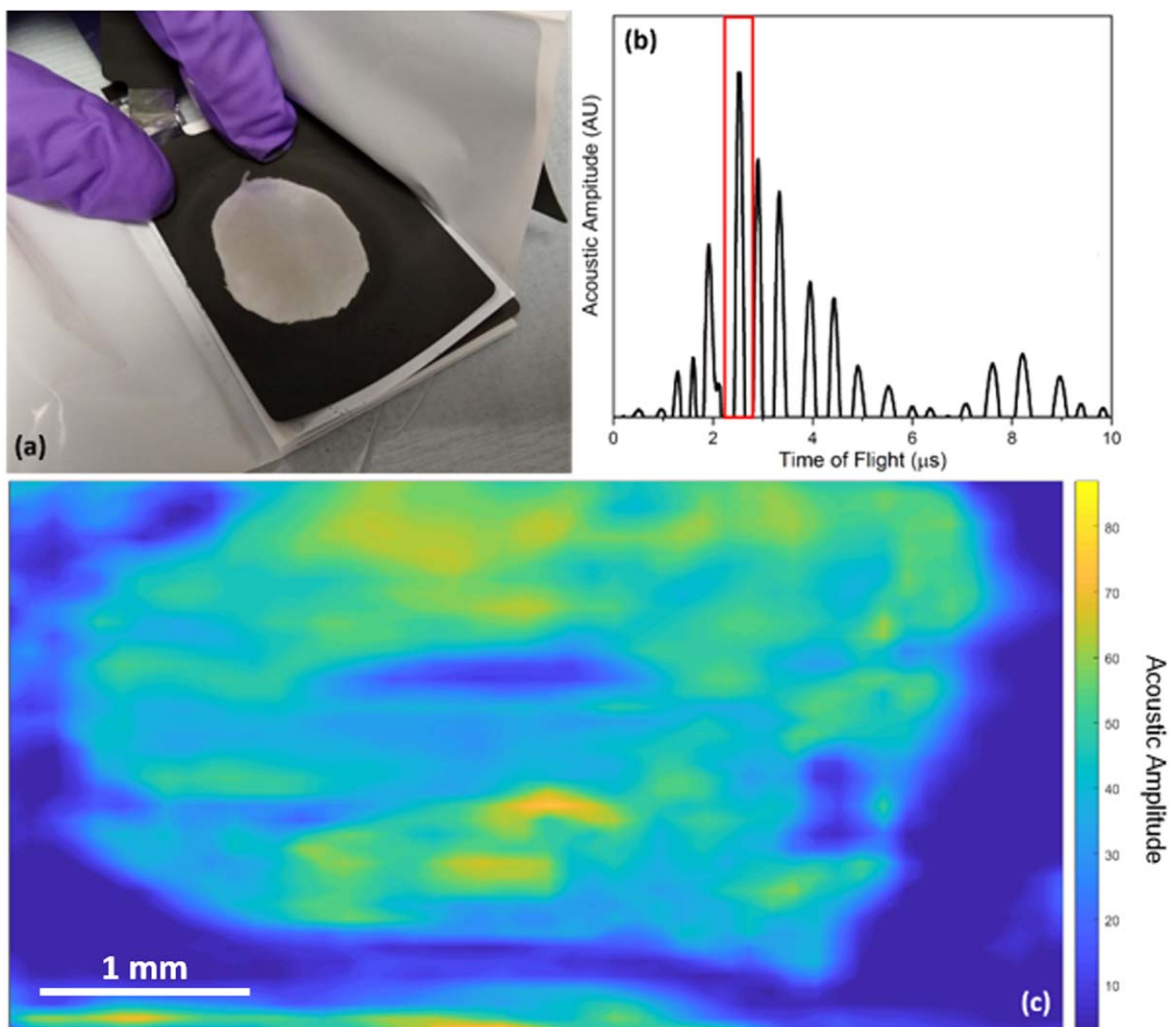


**Figure 4.** Diagnostic approach to identifying defects in cathode deposition (a) shown in a photograph prior to cell sealing (b) a single acoustic scan highlighting the ToF peak of interest at 2.5  $\mu\text{s}$  and (c) a 2D raster showing a region corresponding to that highlighted in the photograph demonstrating the efficacy of the technique.

Figure 4 shows the amplitude of the peak that can be ascribed to the interface of the electrolyte and bare current collector; the apparently reduced amplitude in the surrounding regions is therefore explained by the scenario shown in Fig. 1a. The image in Fig. 4c was obtained similarly to that shown in Fig. 2b with a candidate peak identified at ca.  $2.5 \mu\text{s}$  analysed across the lateral extent of the defective battery. A region corresponding to the defect shown in Fig. 4a can clearly be seen, with this area also correlating a variation in amplitude of the fourth significant peak and therefore the defect located in the fourth layer. Variations in the amplitude can be observed across the defect, with this ascribed to pressure variations as the transducer is rastered across the surface of the battery. The demonstration of this technique to detect defects at resolutions below the electrode thickness indicates significant promise for the deployment of acoustic techniques as a tool for both in-line QA of coating processes, by imaging the underside of coated electrodes, and as a final QC metric for cell assembly. Indeed, given the ongoing improvement in X-ray imaging times, ultrasonic measurements could be used as a preliminary screening technique as part of a wider triage process to mitigate against cell defects, preventing catastrophic failures and associated economic costs for cell manufacturers.

While the validation of defects on a millimetre scale has an impact for the in-line deployment of ultrasonic ToF techniques, the identification of foreign artefacts, localised defects or delamination at a micrometre scale would allow the technique to be deployed to a wider range of users. Commercial cells are more finely optimised for performance, and, as a result are typically more rigid and contain less electrolyte than lab-built pouch cells. The scale of defects which are most likely to arise in commercial cells would be expected to be smaller than the diameter of a transducer; and therefore, unlikely to result in measureable variations in electrode location. As such, a single transducer placed in the correct location is likely to be sufficient to capture the effect of defects. However, it should be highlighted that architectural features and large defects may extend beyond the scope of a single transducer, and, defects may occur at any position in the cell emphasising the need for spatially resolved examinations.<sup>30</sup> To investigate the application of this technique to a commercial cell, two 400 mAh batteries, one pristine and one with a defect, were examined, with the results shown in Fig. 5.

The ultrasonic waveform associated with the pristine cell in Fig. 5a is indicative of the regular layered structure expected in a Li-ion pouch cell, as seen in Fig. 5c. The signals obtained in the pristine commercial cell can be seen to be more homogenous than those obtained in the lab-built cell highlighting the potential use of this technique as a QA/QC diagnostic. As previously highlighted, deviations from this structure have been associated with capacity fade and cell failure<sup>13,14,16</sup> making such deviations a candidate metric to interrogate the SoH of batteries. The waveform acquired from the defective cell (Fig. 5b) shows significant variations from the pristine waveforms at ToF above ca.  $1.25 \mu\text{s}$  suggesting the defect is located in the region of this ToF. It should be noted that in contrast to the previous results no delay block was used in this instance so the initial signal contains peaks associated with the ringing of the transducer. The absolute amplitude and periodicity of the signal is observed to decrease substantially throughout the primary signal in Fig. 5b alongside the disappearance of the first and second echo peaks located at ca. 6 and 11  $\mu\text{s}$ , respectively. The absence of these echo peaks suggests that the waveform is not able to propagate through the cell to the rear casing and back to the transducer due to some form of defect. While no macroscale gassing of the cell was observed prior to measurement the presence of gas in the region adjacent to the defect cannot be ruled out and may explain the substantial drop in signal propagation beyond the defect. Having obtained this waveform, the cell was examined using high-resolution X-ray CT to understand the cause of the signal attenuation. Once reconstructed, a single defect was identified in the second cathode layer, as highlighted in Fig. 5. The nature of this defect could not be fully determined; however, it was observed to be ca.  $20 \mu\text{m}$  in diameter. Secondary effects of this defect were noticed in a  $200 \mu\text{m}$

radial region (highlighted in blue boxes in Figs. 5d, 5e) in the electrode plane with a small increased distance ( $>5 \mu\text{m}$ ) observed between the second anode and cathode layers. It is suggested that this increased distance introduced an acoustically resistive void, which affected the propagation pathway for the acoustic signal resulting in a large acoustic impedance and consequently a high degree of signal attenuation. In this instance, the peaks located after the signs of degradation may correspond to echo reflections, which manifest between the transducer and the defective layer due to the large reflection coefficient (described in Eq. 6) at the electrode/void interface. These peaks may also arise due to reflections that occur beyond the defect with a significantly attenuated signal.

To confirm this hypothesis the transmission of acoustic waves through the pristine and defective cells was investigated using two transducers as explained previously, with the results shown in Fig. 6. It is evident that the presence of the internal defect significantly retards the transmission of an acoustic wave through the battery. The high amplitude transmission peak, which begins at ca.  $2.5 \mu\text{s}$  in the pristine cell, is not present in the defective cell, with subsequent peaks also not observed. It can also be seen that the signal recorded contains significantly fewer component peaks. The substantially reduced transmission of the acoustic signal provides further evidence as to the presence of an acoustically insulating layer suggesting the defect observed in Figs. 5d, 5e resulted in a separation of the component layers, through either physical means or the formation of a layer of gas.

The use of pulse-echo techniques has been shown to provide depth-resolution, offering the opportunity to pinpoint the location of defects in cells. However, the technique must be tailored for the appropriate thickness range to ensure the received signal is sufficiently large to be recorded while also not exceeding the maximum amplitude recordable by the transducer. This limitation could be overcome by recording the response to sequential pulses of varying amplitude to probe a range of depths. The use of acoustic transmission techniques to identify defects has been shown to have the advantage of a more facile analysis; however, the technique does not provide information relating to the internal structure of the cell. It is also likely that transmission measurements would provide a simpler correlative tool for the identification of voids caused by either gas or defect formation in cells with no need for *a priori* knowledge of cell componentry or condition. The optimised nature of commercial cells, with a minimal electrolyte volume will also aid the use of this technique when compared to lab-built cells.

## Conclusions

Acoustic pulse-echo spectroscopy was performed on lab-built cells with in-built defects and on pristine and defective commercially available cells, with acoustic transmission used to corroborate the presence of such defects. These measurements were further validated using X-ray computed tomography to highlight the potential of acoustic measurements as a quality assurance and quality control tool in manufacturing, operational and end-of-life scenarios. The presence of defects were clearly identifiable in the characteristic ultrasonic waveforms with the importance of spatial resolution highlighted in the lab-built cells, where the defects were sufficiently large to result in widespread variability in the cell condition. The microscale defect observed in the commercial cell was sufficiently characterised using a single transducer providing a pathway for direct SoH monitoring in Li-ion cells.

The techniques described in this work benefit from the relatively compact, low-cost nature of the componentry, in addition to rapid data acquisition, which offer the potential to form part of an in-line QA triage system to identify potentially problematic cells in real-time prior to deeper analysis using complimentary methodologies. Acoustic spectroscopy may further substantially enhance SoH monitoring of batteries, with the time-series information currently being readily analysed by on-board BMSs in a wide array of Li-ion battery packs. Furthermore the application of frequency domain

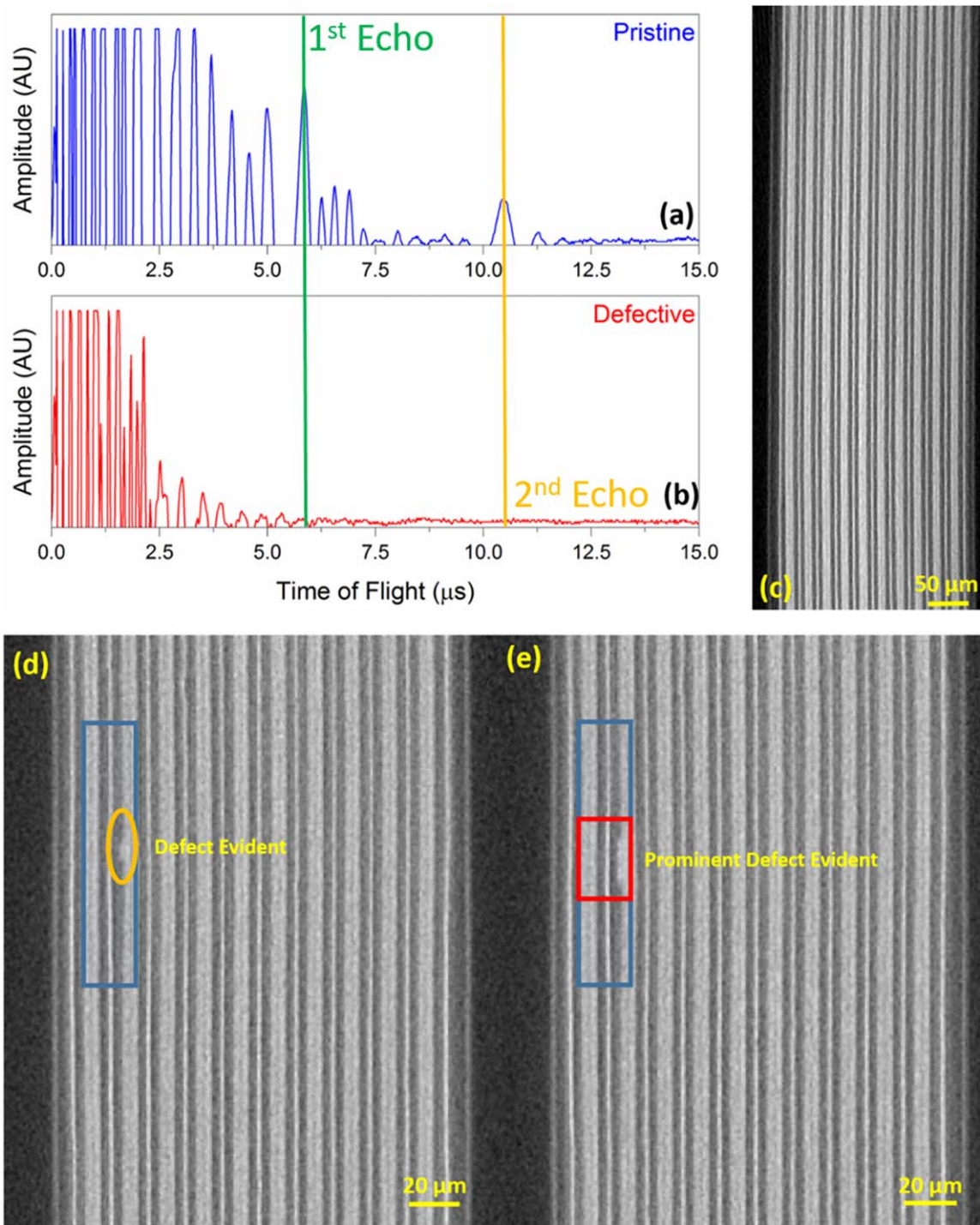


**Figure 5.** Identifying microscale defects in commercial pouch cells using ultrasound pulse-echo techniques. The spectra associated with pristine (a) and defective (b) cells are shown, with a reconstructed X-ray tomography slice of the pristine cell shown in (c). Following the identification of a suspected defect using ultrasound techniques the cell was examined using X-ray tomography with the presence of a single defect in the cell confirmed, as shown in (d), (e).

analysis may facilitate layer-wise reconstructions which could be a powerful addition to battery monitoring systems in certain applications. The application of this technique as a correlative tool to identify deviations from expected behaviour could also be used as a first step in end-of-life assessment for batteries, aiding the ever-increasing drive to improve the reusability, remanufacture and recycling of Li-ion cells and components.

#### Acknowledgments

The authors would like to acknowledge the EPSRC for supporting the energy storage work in the Electrochemical Innovation Lab (EP/R020973/1; EP/R023581/1; EP/N032888/1) and the Institute for Future Transport and Cities (EP/R023581/1) and Innovate UK for funding the ‘Valuable’ project (Grant No. 104182). The authors would also like to acknowledge the Royal Academy of Engineering for funding Robinson and Shearing through ICRF1718\1\34 and CiET1718 respectively and the Faraday Institution (EP/S003053/1, grants FIRG003, FIRG014).

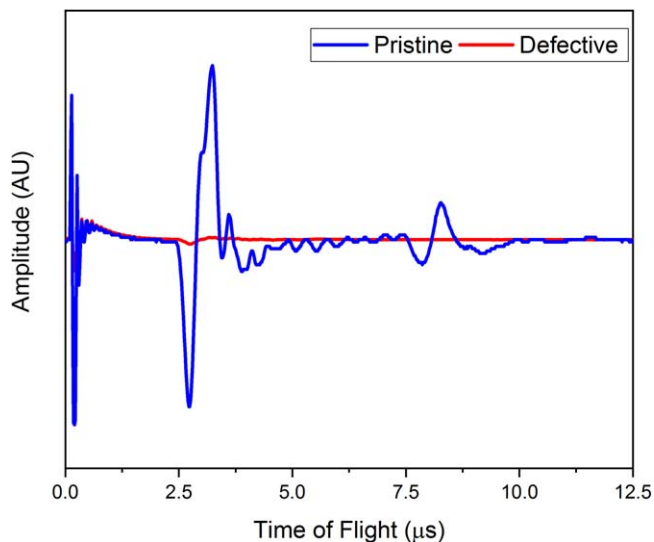


**Figure 6.** Ultrasonic ToF waveforms obtained through transmission mode through the pristine and defective commercial cells shown in Fig. 5 showing large differences between the transmission signals due to the presence of the defect.

The authors also acknowledge the STFC for supporting Shearing and Brett (ST/K00171X/1) and ACEA for supporting ongoing research at the EIL. Support from the National Measurement System of the UK Department for Business, Energy and Industrial Strategy is also gratefully acknowledged.

### ORCID

James B. Robinson <https://orcid.org/0000-0002-6509-7769>  
 Rhodri E. Owen <https://orcid.org/0000-0002-1246-2988>  
 Matt D. R. Kok <https://orcid.org/0000-0001-8410-9748>  
 Jude Majasan <https://orcid.org/0000-0002-9573-5039>  
 Tazdin Amietszajew <https://orcid.org/0000-0001-7452-1034>  
 Alexander J. Roberts <https://orcid.org/0000-0002-3920-9579>  
 Jarred Z. Olson <https://orcid.org/0000-0001-7560-8668>  
 Dan J. L. Brett <https://orcid.org/0000-0002-8545-3126>  
 Paul R. Shearing <https://orcid.org/0000-0002-1387-9531>

### References

1. Japan Transport Safety Board, *Aircraft Serious Incident Investigation Report All Nippon Airways Co., LTDJA804A. Report No. AI2014-4* (2014), [https://www.mlit.go.jp/jtsb/eng-air\\_report/JA804A.pdf](https://www.mlit.go.jp/jtsb/eng-air_report/JA804A.pdf).
2. U.S. Department of Energy, *Report of Investigation: Hybrids Plus Plug in Hybrid Electric Vehicle* (2008), <https://prius-touring-club.com/librairie/mediateque/pdf/toyota-prius-a123-car-fire-investigation-report-2008.pdf>.
3. Air Accident Investigation Branch, *Report on the serious incident to Boeing B787-8, ET-AOP London Heathrow Airport on 12 July 2013* (2015), [https://assets.publishing.service.gov.uk/media/55d43f8d40f0b6091a000001/AAIB\\_2-2015\\_ET-AOP.pdf](https://assets.publishing.service.gov.uk/media/55d43f8d40f0b6091a000001/AAIB_2-2015_ET-AOP.pdf).
4. National Transport Safety Board, *Auxiliary Power Unit Battery Fire Japan Airlines Boring 787-8, JA829J Report No. NTSB/AIR-14/01* (2014), <https://www.ntsb.gov/investigations/AccidentReports/Reports/AIR1401.pdf>.
5. M. J. Loveridge et al., "Looking deeper into the Galaxy (Note 7)." *Batteries*, **4**, 1 (2018).
6. Samsung, (2016), Samsung Expands Recall to All Galaxy Note7 Devices <https://pages.samsung.com/us/note7recall/index.jsp>.
7. Shmuel De-Leon, *Samsung Galaxy Note7 Case—Battery Safety Issues Impact on Business* (2017), <http://www.sdle.co.il/wp-content/uploads/2018/08/18-samsung-case-battery-safety-issues-impact-on-business-ver-3.pdf>.
8. M. Broussely, P. Biensan, F. Bonhomme, P. Blanchard, S. Herreyre, K. Nechev, and R. J. Staniewicz, "Main aging mechanisms in Li ion batteries." *J. Power Sources*, **146**, 90 (2005).
9. Y. Zhang, C. Zhao, and Z. Guo, "Simulation of crack behavior of secondary particles in Li-ion battery electrodes during lithiation/de-lithiation cycles." *Int. J. Mech. Sci.*, **155**, 178 (2019).
10. J. Li, E. Murphy, J. Winnick, and P. Kohl, "Studies on the cycle life of commercial lithium ion batteries during rapid charge–discharge cycling." *J. Power Sources*, **102**, 294 (2001).
11. B. Lu, C. Ning, D. Shi, Y. Zhao, and J. Zhang, "Review on electrode-level fracture in lithium-ion batteries." *Chinese Phys. B.*, **29**, 026201 (2020).
12. J. P. Pender et al., "Electrode degradation in lithium-ion batteries." *ACS Nano*, **14**, 1243 (2020).
13. A. Pfrang, A. Kersys, A. Kriston, D. U. Sauer, C. Rahe, S. Käbitz, and E. Figgemeier, "Long-term cycling induced jelly roll deformation in commercial 18650 cells." *J. Power Sources*, **392**, 168 (2018).
14. T. Waldmann, S. Gorse, T. Samtleben, G. Schneider, V. Knoblauch, and M. Wohlfahrt-Mehrens, "A mechanical aging mechanism in lithium-ion batteries." *J. Electrochem. Soc.*, **161**, A1742 (2014).
15. J. Kurfer, M. Westermeier, C. Tammer, and G. Reinhart, "Production of large-area lithium-ion cells—preconditioning, cell stacking and quality assurance." *CIRP Ann.*, **61**, 1 (2012).
16. M. D. R. Kok, J. B. Robinson, J. S. Weaving, A. Jnawali, M. Pham, F. Iacoviello, D. J. L. Brett, and P. R. Shearing, "Virtual unrolling of spirally-wound lithium-ion cells for correlative degradation studies and predictive fault detection." *Sustain. Energy Fuels*, **3**, 2972 (2019).
17. J. Zhang and J. Lee, "A review on prognostics and health monitoring of Li-ion battery." *J. Power Sources*, **196**, 6007 (2011).
18. X. Li, C. Yuan, X. Li, and Z. Wang, "State of health estimation for Li-Ion battery using incremental capacity analysis and Gaussian process regression." *Energy*, **190**, 116467 (2020).
19. L. Chen, Z. Lü, W. Lin, J. Li, and H. Pan, "A new state-of-health estimation method for lithium-ion batteries through the intrinsic relationship between ohmic internal resistance and capacity." *Measurement*, **116**, 586 (2018).
20. M. Berecibar, F. Devriendt, M. Dubarry, I. Villarreal, N. Omar, W. Verbeke, and J. Van Mierlo, "Online state of health estimation on NMC cells based on predictive analytics." *J. Power Sources*, **320**, 239 (2016).
21. G. You, S. Park, and D. Oh, "Real-time state-of-health estimation for electric vehicle batteries: a data-driven approach." *Appl. Energy*, **176**, 92 (2016).
22. X. Hu, J. Jiang, D. Cao, and B. Egardt, "Battery health prognosis for electric vehicles using sample entropy and sparse Bayesian predictive modeling." *IEEE Trans. Ind. Electron.*, **63**, 2645 (2016).
23. Y. Zou, X. Hu, H. Ma, and S. E. Li, "Combined state of charge and state of health estimation over lithium-ion battery cell cycle lifespan for electric vehicles." *J. Power Sources*, **273**, 793 (2015).
24. T. Ohzuku, H. Tomura, and K. Sawai, "Monitoring of particle fracture by acoustic emission during charge and discharge of Li/MnO<sub>2</sub> cells." *J. Electrochem. Soc.*, **144**, 3496 (1997).
25. C. Villeveille, M. Boinet, and L. Monconduit, "Direct evidence of morphological changes in conversion type electrodes in Li-ion battery by acoustic emission." *Electrochem. Commun.*, **12**, 1336 (2010).
26. K. Rhodes, N. Dudney, E. Lara-Curzio, and C. Daniel, "Understanding the degradation of silicon electrodes for lithium-ion batteries using acoustic emission." *J. Electrochem. Soc.*, **157**, A1354 (2010).
27. B. Sood, C. Hendricks, M. Osterman, and M. Pecht, "Health monitoring of lithium-ion batteries." *Electron. Device Fail. Anal.*, **16**, 4 (2014).
28. A. G. Hsieh, S. Bhadra, B. J. Hertzberg, P. J. Gjeltema, A. Goy, J. W. Fleischer, and D. A. Steingart, "Electrochemical-acoustic time of flight: in operando correlation of physical dynamics with battery charge and health." *Energy Environ. Sci.*, **8**, 1569 (2015).
29. G. Davies, K. W. Knehr, B. Van Tassell, T. Hodson, S. Biswas, A. G. Hsieh, and D. A. Steingart, "State of charge and state of health estimation using electrochemical acoustic time of flight analysis." *J. Electrochem. Soc.*, **164**, A2746 (2017).
30. J. B. Robinson, M. Maier, G. Alster, T. Compton, D. J. L. Brett, and P. R. Shearing, "Spatially resolved ultrasound diagnostics of Li-ion battery electrodes." *Phys. Chem. Chem. Phys.*, **21**, 6354 (2019).
31. J. B. Robinson, M. Pham, M. D. R. Kok, T. M. M. Heenan, D. J. L. Brett, and P. R. Shearing, "Examining the cycling behaviour of li-ion batteries using ultrasonic time-of-flight measurements." *J. Power Sources*, **444**, 227318 (2019).
32. C. Bommier, Y. Lu, M. Williams, C. Bommier, W. Chang, Y. Lu, J. Yeung, and G. Davies, "In operando acoustic detection of lithium metal plating in commercial LiCoO<sub>2</sub>/graphite pouch cells." *Cell Reports Phys. Sci.*, **1**, 100035 (2020).